Astronomy & Astrophysics manuscript no. 47˙T
October 3, 2014
© ESO 2014

arXiv:1410.0536v1 [astro-ph.GA] 2 Oct 2014

The white dwarf cooling sequence of 47 Tucanae

Enrique García–Berro[1,2], Santiago Torres[1,2], Leandro G. Althaus[3,4], and Marcelo M. Miller Bertolami[4,5,6]

[1] Departament de Física Aplicada, Universitat Politècnica de Catalunya, c/Esteve Terrades 5, 08860 Castelldefels, Spain
[2] Institute for Space Studies of Catalonia, c/Gran Capita 2–4, Edif. Nexus 104, 08034 Barcelona, Spain
[3] Facultad de Ciencias Astronómicas y Geofísicas, Universidad Nacional de La Plata, Paseo del Bosque s/n, 1900 La Plata, Argentina
[4] Instituto de Astrofísica de La Plata, UNLP-CONICET, Paseo del Bosque s/n, 1900 La Plata, Argentina
[5] Max-Planck-Institut für Astrophysik, Karl-Schwarzschild Strasse 1, 85748 Garching, Germany
[6] Post-doctoral Fellow of the Alexander von Humboldt Foundation

October 3, 2014

Abstract

Context. 47 Tucanae is one of the most interesting and well observed and theoretically studied globular clusters. This allows us to study the reliability of our understanding of white dwarf cooling sequences, to confront different methods to determine its age, and to assess other important characteristics, like its star formation history.
Aims. Here we present a population synthesis study of the cooling sequence of the globular cluster 47 Tucanae. In particular, we study the distribution of effective temperatures, the shape of the color-magnitude diagram, and the corresponding magnitude and color distributions
Methods. We do so using an up-to-date population synthesis code based on Monte Carlo techniques, that incorporates the most recent and reliable cooling sequences and an accurate modeling of the observational biases.
Results. We find a good agreement between our theoretical models and the observed data. Thus, our study, rules out previous claims that there are still missing physics in the white dwarf cooling models at moderately high effective temperatures. We also derive the age of the cluster using the termination of the cooling sequence, obtaining a good agreement with the age determinations using the main-sequence turn-off. Finally, we find that the star formation history of the cluster is compatible with that obtained using main sequence stars, which predict the existence of two distinct populations.
Conclusions. We conclude that a correct modeling of the white dwarf population of globular clusters, used in combination with the number counts of main sequence stars provides an unique tool to model the properties of globular clusters.

Key words. stars: white dwarfs – stars: luminosity function, mass function – (Galaxy:) globular clusters: general – (Galaxy:) globular clusters: individual (NGC 104, 47 Tuc)

1. Introduction

White dwarfs are the most usual stellar evolutionary end-point, and as such they convey important and valuable information about their parent populations. Moreover, their structure and evolutionary properties are well understood – see, for instance Althaus et al. (2010) for a recent review – and their cooling times are, when controlled physical inputs are adopted, as reliable as main sequence lifetimes (Salaris et al. 2013). These characteristics have allowed the determination of accurate ages using the termination of the degenerate sequence for both open and globular clusters. This includes, to cite a few examples, the old, metal-rich open cluster NGC 6791 (García-Berro et al. 2010) which has two distinct termination points of the cooling sequence (Bedin et al. 2005, 2008a,b), the young open clusters M 67 (Bellini et al. 2010) and NGC 2158 (Bedin et al. 2010), or the globular clusters M4 (Hansen et al. 2002) and NGC 6397 (Hansen et al. 2013). However, the precise shape of the cooling sequence also carries important information about the individual characteristics of these clusters, and moreover can help in checking the correctness of the theoretical white dwarf evolutionary sequences. Recently, some concerns – based on the degenerate cooling sequence of the globular cluster 47 Tuc – have been raised about the reliability of the available cooling sequences (Goldsbury et al. 2012). 47 Tuc is a metal-rich globular cluster, being its metallicity [Fe/H]= -0.75 or, equivalently, $Z \approx 0.003$. Thus, there exist accurate cooling ages and progenitor evolutionary times of the appropriate metallicity (Renedo et al. 2010). Hence, this cluster can be used as a testbed for studying the accuracy and correctness of the theory of white dwarf evolution. Estimates of its age can be obtained fitting the main-sequence turnoff, yielding values ranging from 10 Gyr to 13 Gyr – see Thompson et al. (2010) for a careful discussion of the ages obtained fitting different sets of isochrones to the main sequence turn off. Additionally, recent estimates based on the location of the faint turn-down of the white dwarf luminosity function give a slightly younger age of 9.9 ± 0.7 Gyr (Hansen et al. 2013). Here we assess the reliability of the cooling sequences using the available observational data. As it will be shown below, the theoretical cooling sequences agree well with this set of data. Having found that the theoretical white dwarf cooling sequences agree with the empirical one we determine the absolute age of 47 Tuc using three different methods, and also we investigate if the recent determinations using number counts of main sequence stars of the star formation history is compatible with the properties of the degenerate cooling sequence of this cluster.

Send offprint requests to: E. García–Berro

2. Observational data and numerical setup

2.1. Observational data

The set of data employed in the present paper is that obtained by Kalirai et al. (2012), which was also employed later by Goldsbury et al. (2012) to perform their analysis. Kalirai et al. (2012) collected the photometry for white dwarfs in 47 Tuc, using 121 orbits of the Hubble Space Telescope (HST). The exposures were taken with the Advanced Camera for Surveys (ACS) and the Wide Field Camera 3 (WFC3), and comprise 13 adjacent fields. A detailed and extensive description of the observations and of the data reduction procedure can be found in Kalirai et al. (2012), and we refer the reader to their paper for additional details.

2.2. Numerical setup

We use an existing Monte Carlo simulator which has been extensively described in previous works (García-Berro et al. 1999; Torres et al. 2002; García-Berro et al. 2004). Consequently, here we will only summarize the ingredients which are most relevant for our work. Synthetic main sequence stars are randomly drawn according to the initial mass function of Kroupa et al. (1993). The selected range of masses is that necessary to produce the white dwarf progenitors of 47 Tuc. In particular, a lower limit of $M > 0.5\,M_{\odot}$ guarantees that enough white dwarfs are produced for a broad range of cluster ages. In our reference model we adopt an age $T_{\rm c} = 11.5$ Gyr, consistent with the main-sequence turn-off age of 47 Tuc – see Goldsbury et al. (2012) and references therein. We also employ the star formation rate of Ventura et al. (2014), which consists in a first burst of star formation of duration $\Delta t = 0.5$ Gyr, followed by a short period of time (~ 0.04 Gyr) during which the star formation activity ceases, and a second short burst of star formation which lasts for ~ 0.06 Gyr. The fraction of white dwarf progenitors that are formed during the first burst of star formation is 25%, whereas the rest of the synthetic stars (75%) – which have a helium enhancement $\Delta Y \sim 0.03$ – are formed during the second one. According to Ventura et al. (2014) the initial first-population in 47 Tuc was about 7.5 times more massive than the cluster current total mass. At present, only 20% of the stars belong to the population with primeval abundances (Milone et al. 2012). Consequently, there is a small inconsistency in the first-to-second generation number ratio employed in our calculations. Since we are trying to reproduce the present-day first-to-second generation ratio, this inconsistency might have consequences in our synthetic luminosity function. To check this we conducted an additional set of calculations varying the percentage of stars with primeval abundances by 5%, and we found that the differences in the corresponding white dwarf luminosity functions were negligible.

Once we know which stars had time to evolve to white dwarfs we compute their photometric properties using the theoretical cooling sequences for white dwarfs with hydrogen atmospheres of Renedo et al. (2010). These cooling sequences are appropriate because the fraction of hydrogen-deficient white dwarfs for this cluster is negligible (Woodley et al. 2012). These evolutionary sequences were evolved self-consistently from the ZAMS, through the giant phase, the thermally pulsing AGB and mass-loss phases, and ultimately to the white dwarf stage, and encompass a wide range of stellar masses – from $M_{\rm ZAMS} = 0.85$ to $5\,M_{\odot}$. To obtain accurate evolutionary ages for the metallicity of 47 Tuc ($Z = 0.003$) we interpolate the cooling ages between the solar ($Z = 0.01$) and subsolar ($Z = 0.001$) values of Renedo et al. (2010). For the second, helium-enhanced, population of synthetic stars we computed a new set of evolutionary sequences which encompass a broad range of helium enhancements. Finally, we also interpolate the white dwarf masses for the appropriate metallicity using the initial-to-final mass relationships of Renedo et al. (2010).

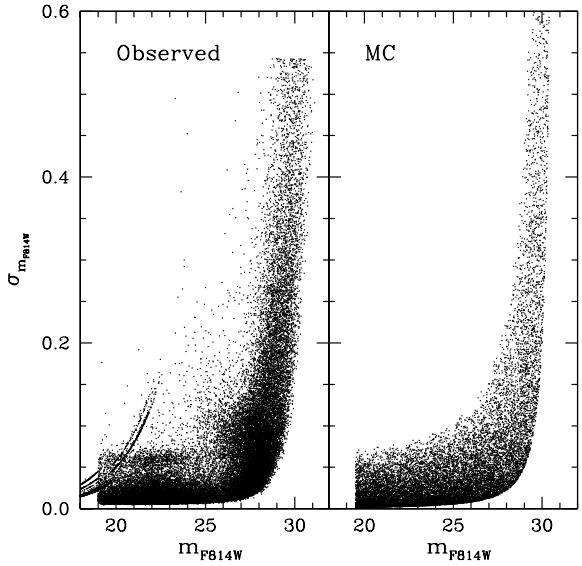

Figure 1. Observed – left panel – and simulated – right panel – distributions of photometric errors. See text for details.

Photometric errors are assigned randomly according to the observed distribution. Specifically, for each synthetic white dwarf the photometric errors are drawn within a hyperbolically increasing band limited by $\sigma_{\rm l} = 0.2\,(m_{\rm F814W} - 31.0)^{-2}$ and $\sigma_{\rm u} = 1.7\,(m_{\rm F814W} - 31.0)^{-2} + 0.06$, which fits well the observations of Kalirai et al. (2012) for the F814W filter. Specifically, the photometric errors are distributed within this band according to the expression $\sigma = (\sigma_{\rm u} - \sigma_{\rm l})x^2$, where $x \in (0, 1)$ is a random number which follows an uniform distribution.. Thus, the photometric errors increase linearly between the previously mentioned boundaries. Similar expressions are employed for the rest of the filters. The observed and simulated photometric errors of a typical Monte Carlo realization are compared in Fig. 1 for the F814W filter. As can be seen in this figure, the observed and the theoretically predicted distribution of errors display a reasonable degree of agreement. In particular, the observed and the theoretical distributions of photometric errors have a relatively broad range of values for F814W ranging from about 20 mag to 25 mag, for which the width of the distribution remains almost flat. However, the width of the distribution increases abruptly for values of F814W larger than this last value.

3. Results

3.1. The empirical cooling curve

To start with, we discuss the distribution of white dwarf effective temperatures, and we compare it with the observed distribution, which is displayed in Fig. 2. Goldsbury et al. (2012) measured the effective temperatures of a large sample of white dwarfs in 47 Tuc. Afterwards they produced a sorted list, from the hottest

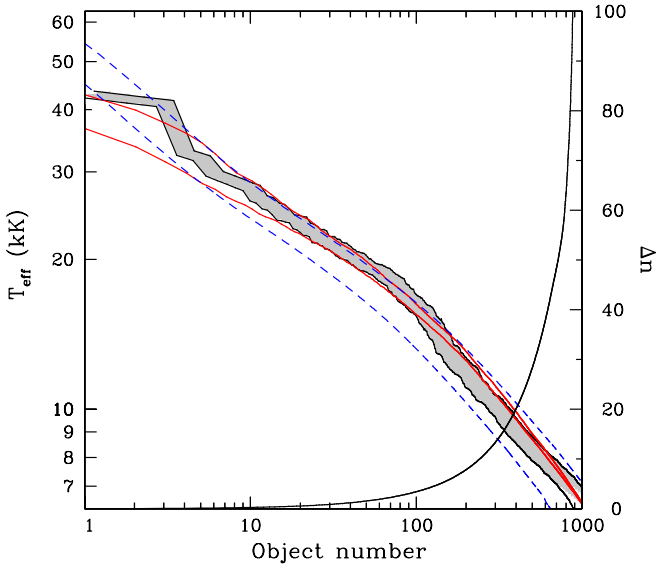

Figure 2. Distribution of effective temperatures as a function of the white dwarf object number (left axis). The observational values of Goldsbury et al. (2012) are displayed using a grey shaded area, while the results of our Monte Carlo simulations are shown using red lines. The blue dashed lines show the cooling sequence for $M_{\rm WD} = 0.53\,M_{\odot}$ of Renedo et al. (2010) for $Z = 0.001$ under different assumptions. The correction factor of the observed sample of white dwarfs is also displayed (right axis). See the online edition of the journal for a color version of this plot.

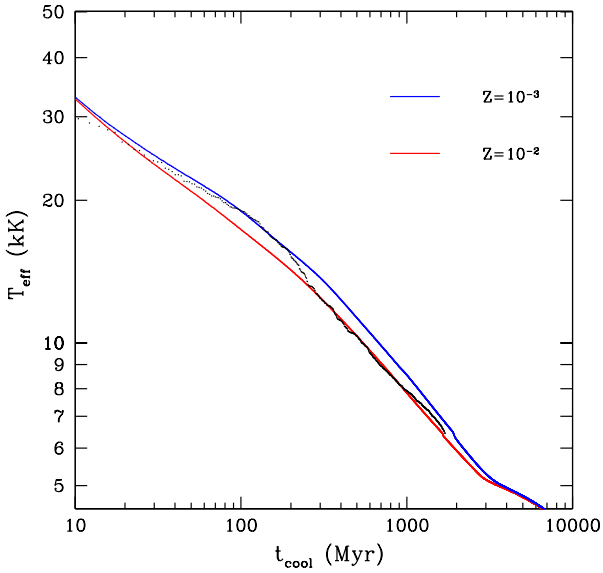

Figure 3. Cooling sequences of Renedo et al. (2010) for the mass of the white dwarf corresponding to the main-sequence turn-off mass, and for two metallicities, compared to the empirical cooling sequence of Goldsbury et al. (2012).

star to the coolest one, to experimentally determine the rate at which white dwarfs are cooling. They assumed a constant white dwarf formation rate. Thus, the position in the sorted list is proportional to the time spent on the cooling sequence. Their sorted, completeness-corrected distribution of effective temperatures is shown Fig. 2 as a grey shaded band, which includes the 1σ statistical errors. Also shown for illustrative purposes is the completeness correction (solid black line).

The most salient feature of the observed distribution is the existence of a pronounced break, which occurs at effective temperatures $T_{\rm eff} = 20,000$ K. This feature remained unexplained in Goldsbury et al. (2012) – see their Fig. 10 – and prompted them to attribute its origin to some missing piece of physics in all the existing models at moderate temperatures. The results of our population synthesis simulations for our reference model are also shown, and also include the 1σ statistical deviations (upper and lower red lines). As can be seen, our calculations are in good agreement with the observed data, without the need of invoking any additional physical mechanism in the cooling sequences, although they do not perfectly match the change in slope of the empirical cooling curve. In the following we discuss separately several possible reasons that may explain why our simulations are in better agreement with the observed distribution than those of Goldsbury et al. (2012).

The first reason that explains why our model better fits the observed list is that we used updated main-sequence lifetimes, the initial-to-final mass relationship of Renedo et al. (2010) for the metallicity of cluster, and interpolated cooling sequences for the precise metallicity of 47 Tuc, while Goldsbury et al. (2012) did not. All this results in a different turn-off mass for the cluster, and consequently in a different white dwarf mass at the top of the cooling sequence, hence in different cooling rates. To assess this, in Fig. 3 the sorted list of Goldsbury et al. (2012) is compared to the theoretical cooling sequences of two white dwarfs of masses $M_{\rm WD} = 0.525\,M_{\odot}$ and $0.520\,M_{\odot}$, the white dwarf mass corresponding to the main-sequence turn-off of 47 Tuc, for two metallicities that embrace the metallicity of the cluster, $Z = 10^{-3}$ and $Z = 10^{-2}$, respectively. It is interesting to note that the $Z = 10^{-3}$ sequence provides a good fit to the empirical cooling sequence of Goldsbury et al. (2012) for temperatures hotter than $T_{\rm eff} = 20,000$ K, while the $Z = 10^{-2}$ sequence is a good fit for temperatures colder than this value. Moreover, the theoretical cooling sequences bracket the observed distribution of effective temperatures, and thus it is not surprising that our simulations fit better the observed distribution. Finally, another explanation for the better fit of our simulations to the observed distribution is that by construction our simulations result in a spread of masses, while Goldsbury et al. (2012) adopted a single cooling track to compare with their observational data.

Nevertheless, although our simulations show an overall good agreement with the observed distribution of effective temperatures, they do not fully reproduce the observed break in the empirical cooling curve at moderately high effective temperatures. We thus explore which is the origin of this discrepancy. Clearly, metallicity cannot be at the origin of the break because in the region of interest the cooling sequences of the white dwarfs corresponding to the main turn-off mass run almost parallel. Also, we adopt the star formation history of Ventura et al. (2014). We repeated our calculations employing a single burst of star formation and the differences were found to be minor. Another possible origin for the break in the observed distribution may be the sudden increase photometric errors for magnitudes larger than 25 – see Fig. 1. We thus checked if the break in the distribu-

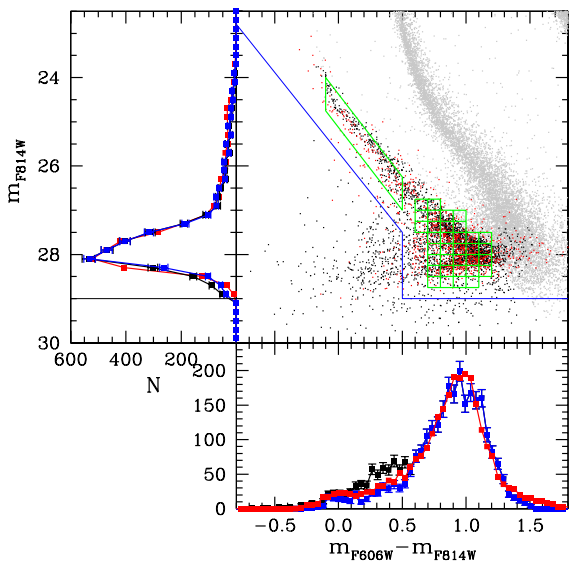

Figure 4. White dwarf luminosity function, color-magnitude diagram and color distribution of 47 Tuc. Grey dots represent observed main sequence stars, black dots correspond to white dwarfs observed in the field, while red points denote the results of our synthetic population of white dwarfs. The green squares represent the regions of the color-magnitude for which the χ^2 test was performed, while the blue thin lines correspond to the cuts adopted to compute the distributions. The red curves correspond to the simulated distributions obtained when no cuts are adopted, the blue ones are the observed distributions computed using our cuts, while the black lines are the observed distributions when no cuts are employed. See the online edition of the journal for a color version of this figure, and the main text for additional details.

tion of observed errors is responsible for the observed break in sorted list, and although the inclusion of realistic photometric errors in the simulated population explains why our model is superior, we found that the observed break cannot be explained by the sudden increase in photometric errors for stars with magnitudes larger than 25 mag. Thus, the reason for the observed break in the empirical curve must be related to either the way the observed data is handled or to an unknown observational bias. We explore these possibilities next.

In Fig. 2 we also show the results of our simulations when we adopt the same procedure used by Goldsbury et al. (2012) – upper blue dashed line. This is equivalent to adopt a single white dwarf cooling sequence of mass $M_{\rm WD} = 0.53\,M_{\odot}$ of a progenitor with metallicity $Z = 0.001$. As can be seen, the first white dwarfs in the cooling curve have effective temperatures larger than $T_{\rm eff} \sim 40,000$ K, whereas in the sorted list of Goldsbury et al. (2012) none is found. If white dwarfs with $T_{\rm eff} \gtrsim 40,000$ K – which have very short evolutionary timescales, and hence are difficult to detect – are removed from the theoretical sorted list the entire distribution is shifted towards the left in this diagram, and we obtain the lower blue dashed line. As can be seen this simple experiment helps in solving the discrepancy found by Goldsbury et al. (2012), although does not totally remove the reported difference. To better assess this, we employ a Kolmogorov-Smirnov test of the cumulative distributions of effective temperatures. We first compute the statistic separation D, which measures the largest separation between the cumulative distribution of our simulations and the observed data. The statistical distances computed in this way are 0.0789 when the Monte Carlo simulation and the observed sorted list are compared, 0.2717 when the model obtained using the procedure of Goldsbury et al. (2012) is compared to the observed the sorted list, and 0.2694 when from this last model the hottest white dwarfs are removed from the sorted list. Using these statistical distances, we compute the probability of the three models being compatible with the observed data. We find that the probability of our Monte Carlo distribution being compatible with the observational one is $P \simeq 0.92$, while this probability drops to $P \simeq 0.73$ when the procedure employed by Goldsbury et al. (2012) is adopted, independently of whether the hottest white dwarfs are removed from the sorted list or not. Thus, although in a strict statistical sense none of the models can be totally excluded to a significant level of confidence – say, for instance, 5% – our population synthesis model presents a better agreement with the observed distribution of effective temperatures, and we judge that there is no reason to invoke a missing piece of physics at moderately high luminosities.

3.2. The color-magnitude diagram

Having assessed the reliability of the theoretical cooling sequences, we now discuss the overall shape of the color-magnitude diagram, and the distributions of magnitudes and colors. All this information is displayed in Fig. 4. The central panel of this figure shows the observed stars, and the synthetic white dwarfs. As can be seen, the distribution of synthetic stars perfectly overlaps with that of observed ones, except at very low luminosities, for which the contamination with galaxies is very likely. For this reason we introduced a magnitude cut at $m_{\rm F814W} = 29$ mag, and we do not consider these objects anymore in the subsequent analysis. Additionally, since we do not have proper motions of the white dwarfs in 47 Tuc, we introduced two more cuts, which are also displayed in this figure. These cuts are also intend to discard all background objects which are not cluster members. In particular, we do not consider objects to the left of F606W−F814W=0.5 mag for magnitudes between 29.0 mag and 27.5 mag, and objects to the left of the line F814W=3.62 ((F606W − F814W) − 0.5) + 27.5 for brighter magnitudes. Since the background contamination is also overimposed to the white dwarf cooling sequence we also estimated the number of background contaminants still present in the green boxes in Fig. 4 . We did this in a statistical way, by assuming that the density of contaminants within these regions is similar to that close to the exclusion line, and we found that the percentage of contamination of each of the green boxes in Fig. 4 is small, ∼ 3%. We then compute the theoretical white dwarf luminosity function, and compare it with the observed luminosity functions when no cuts are employed, and when the color and magnitude cuts are used. Note that the differences between the two observed luminosity functions are neglibible for magnitudes brighter than that of the peak at ∼ 28 mag, and very small for fainter magnitudes. Moreover, the agreement between theory and observations is again excellent. We emphasize that should some physics was missing in the theoretical cooling tracks we would not be able to obtain such a good agreement at high luminosities. Finally, the bottom panel of this figure shows the color distributions. Again, the agreement is very good, except for the presence of a small bump in the observed distribution at F606W−F814W∼ 0.3 mag

when no cuts are used. However, when we discard the sources that very likely are not cluster white dwarfs the agreement is excellent.

As mentioned, the white dwarf cooling sequence of 47 Tuc carries interesting information about its star formation history and age. To derive this information we use the following approach. We compute independent χ^2 tests for the magnitude ($\chi^2_{\rm F814W}$) and color ($\chi^2_{\rm F606W-F814W}$) distributions. Additionally, we calculate the number of white dwarfs inside each of the green boxes in the color-magnitude diagram of Fig. 4 – which are the same regions of this diagram used by Hansen et al. (2013) to compare observations and simulations – and we perform an additional χ^2 test, χ^2_N. We then investigate which are the values of the several parameters which define the star formation history of the cluster – that is, its age, the duration of the two bursts, and their separation – that best fit the observed data, independently. That is, we seek for the parameters of the star formation history of 47 Tuc that best fit either the white dwarf luminosity function, or the color distribution or the number of stars in each of the boxes in Fig. 4. Obviously, this procedure results in different values of the parameters that define the star formation history of 47 Tuc.

The results of our analysis are shown in Table 1, where only the data for a reduced set of models in which we kept fixed the separation between the two bursts of star formation and the duration of the second burst, and varied the age of the cluster and the duration of the first burst, is listed. We remark, nonetheless, that we explored a significantly larger range of parameters, and that for the sake of conciseness we only show here a few models. We do this because we find that the values of χ^2 are less sensitive to variations in the rest of parameters, and thus this set of models turns out to be quite representative. As can be seen, when the white dwarf luminosity function is employed to obtain the age of the cluster and the duration of the burst of star formation the χ^2 test favors an age $T_{\rm c} \simeq 12.5 \pm 1.0$ Gyr and a duration $\Delta t \simeq 1.0 \pm 0.5$ Gyr. Instead, when the color distribution is employed we obtain $T_{\rm c} \simeq 11.5 \pm 1.0$ Gyr and $\Delta t \simeq 0.6 \pm 0.5$ Gyr, respectively, while the model that best fits the number of stars in each bin of the color-magnitude diagram has an age $T_{\rm c} \simeq 12.5 \pm 0.5$ Gyr and a duration of the burst of star formation $\Delta t \simeq 0.7 \pm 0.5$ Gyr. These results are in accordance with those of Ventura et al. (2014), agree with the absolute age determination of 47 Tuc using the eclipsing binary V69 (Thompson et al. 2010), and also agreee each other within the error bars.

4. Conclusions

In this paper we have assessed the reliability and accuracy of the available cooling tracks using the white dwarf sequence of 47 Tuc. We have demonstrated that when the correct set of evolutionary sequences of the appropriate metallicity are employed, and a correct treatment of the photometric errors, and observational biases is done, the agreement between the observed and simulated distributions of effective temperatures, magnitudes and colors, as well as the general appearance of the color-magnitude diagram is excellent, without the need of invoking any missing piece of physics at moderately high effective temperatures in the cooling sequences. While our models do not totally reproduce the sudden change of slope in the empirical cooling sequence, it is worth noting that such change of slope takes place in the region where the completeness correction factor becomes relevant. Thus it might be well possible that this feature may be only due to some unknown observational bias.

In a second phase, and given that we found that there is no reason to suspect the theoretical cooling sequences are incomplete, we also used these distributions to study the age and star formation history of the cluster using three different distributions: the white dwarf luminosity function, the color distribution, and the number counts of stars in the color-magnitude diagram. Using these three methods we obtained that the age of the cluster is $T_{\rm c} \sim 12.0$ Gyr. Our results are compatible with the recent results of Ventura et al. (2014), who found that star formation in this cluster proceeded through two bursts, the first one of duration ~ 0.4 Gyr, while the second one lasted for ~ 0.06 Gyr, separated by a gap of duration ~ 0.04 Gyr. We also found that the relative strengths of these bursts of star formation activity (25% and 75%, respectively), and the presence of a helium-enhanced population of white dwarf progenitors (born exclusively during the second burst) are also compatible with the characteristics of the white dwarf population.

Since our analysis of the cooling sequence of 47 Tuc closely agrees with what is obtained studying the distribution of main-sequence stars, we conclude that a combined strategy provides a powerful tool that can be used to study other star clusters, and from this obtain important information about our Galaxy. In these sense, it is important to realize that Hansen et al. (2013) computed the age of NGC 6397, obtaining $\sim$ 12 Gyr, significantly longer than their computed age for 47 Tuc ($\sim$ 10 Gyr). This prompted them to suggest that there is quantitative evidence that metal-rich clusters like 47 Tuc formed later than the metal-poor halo clusters like NGC 6397. Our study indicates that 47 Tuc is older than previously thought, and consequently, although this may be true, more elaborated studies are needed.

Acknowledgements. This work was partially supported by MCINN grant AYA2011–23102 by the European Union FEDER funds, by AGENCIA through the Programa de Modernización Tecnológica BID 1728/OC-AR, and by PIP 112-200801-00940 grant from CONICET. We thank R. Goldsbury and B.M.S. Hansen for providing us with the observational data shown in Figs. 2 and 4.

References

Althaus, L. G., Córsico, A. H., Isern, J., & García-Berro, E. 2010, A&A Rev., 18, 471
Bedin, L. R., King, I. R., Anderson, J., et al. 2008a, ApJ, 678, 1279
Bedin, L. R., Salaris, M., King, I. R., et al. 2010, ApJ, 708, L32
Bedin, L. R., Salaris, M., Piotto, G., et al. 2008b, ApJ, 679, L29
Bedin, L. R., Salaris, M., Piotto, G., et al. 2005, ApJ, 624, L45
Bellini, A., Bedin, L. R., Piotto, G., et al. 2010, A&A, 513, A50
García-Berro, E., Torres, S., Althaus, L. G., et al. 2010, Nature, 465, 194
García-Berro, E., Torres, S., Isern, J., & Burkert, A. 1999, Month. Not. Roy. Astron. Soc., 302, 173
García-Berro, E., Torres, S., Isern, J., & Burkert, A. 2004, Astron. & Astrophys., 418, 53
Goldsbury, R., Heyl, J., Richer, H. B., et al. 2012, ApJ, 760, 78
Hansen, B. M. S., Brewer, J., Fahlman, G. G., et al. 2002, ApJ, 574, L155
Hansen, B. M. S., Kalirai, J. S., Anderson, J., et al. 2013, Nature, 500, 51
Kalirai, J. S., Richer, H. B., Anderson, J., et al. 2012, AJ, 143, 11
Kroupa, P., Tout, C. A., & Gilmore, G. 1993, MNRAS, 262, 545
Milone, A. P., Piotto, G., Bedin, L. R., et al. 2012, ApJ, 744, 58
Renedo, I., Althaus, L. G., Miller Bertolami, M. M., et al. 2010, Astrophys. J., 717, 183
Salaris, M., Althaus, L. G., & García-Berro, E. 2013, A&A, 555, A96
Thompson, I. B., Kaluzny, J., Rucinski, S. M., et al. 2010, AJ, 139, 329
Torres, S., García-Berro, E., Burkert, A., & Isern, J. 2002, MNRAS, 336, 971
Ventura, P., Criscienzo, M. D., D'Antona, F., et al. 2014, MNRAS, 437, 3274
Woodley, K. A., Goldsbury, R., Kalirai, J. S., et al. 2012, AJ, 143, 50

Table 1. χ^2 test of the luminosity function, color distribution and color-magnitude diagram, for different ages and durations of the first burst of star formation. We list the normalized value of χ^2, that is the value of χ^2 over its minimum value.

	$\chi^2_{\rm F814W}/\chi^2_{\rm min}$				$\chi^2_{\rm F606W-F814W}/\chi^2_{\rm min}$				$\chi^2_{\rm N}/\chi^2_{\rm min}$			
T_c (Gyr)	Δt (Gyr)											
	0.25	0.50	0.75	1.0	0.25	0.50	0.75	1.0	0.25	0.50	0.75	1.0
10.0	3.21	3.95	4.58	5.56	1.76	1.91	2.15	2.66	9.81	11.47	12.28	13.97
10.5	1.96	2.44	2.97	3.57	1.29	1.44	1.63	1.81	5.93	7.67	9.22	10.46
11.0	1.42	1.62	1.92	2.30	1.16	1.17	1.31	1.42	3.46	4.26	5.70	6.96
11.5	1.25	1.27	1.33	1.42	1.00	1.00	1.03	1.10	1.49	2.08	2.95	3.81
12.0	1.17	1.10	1.10	1.18	1.17	1.05	1.03	1.07	1.17	1.20	1.43	2.04
12.5	1.53	1.35	1.13	1.00	1.59	1.39	1.14	1.11	1.49	1.31	1.00	1.19
13.0	1.97	1.78	1.43	1.29	1.90	1.67	1.53	1.36	2.13	1.97	1.50	1.37